Exp Astron
DOI 10.1007/s10686-012-9298-x

ORIGINAL ARTICLE

Sub-electron readout noise in a Skipper CCD fabricated on high resistivity silicon

Guillermo Fernández Moroni · Juan Estrada · Gustavo Cancelo · Stephen E. Holland · Eduardo E. Paolini · H. Thomas Diehl

Received: 22 September 2011 / Accepted: 18 March 2012

Abstract The readout noise for Charge-Coupled Devices (CCDs) has been the main limitation when using these detectors for measuring small amplitude signals. A scientific CCD fabricated on a high-resistivity silicon substrate utilizing a floating gate amplifier with the capability of multiple sampling of the charge signal is described in this paper. The Skipper CCD architecture and its

G. Fernández Moroni (✉) · E. E. Paolini
Inst. de Inv. en Ing. Eléctrica (IIIE) "Alfredo C. Desages", Dto. Ing. Eléctrica Comp., Universidad Nacional del Sur, Av. Alem 1253 - (B8000CPB) Bahía Blanca, Buenos Aires, Argentina
e-mail: gfmoroni@fnal.gov

E. E. Paolini
e-mail: epaolini@uns.edu.ar

G. Fernández Moroni · J. Estrada · G. Cancelo · H. T. Diehl
Fermi National Accelerator Laboratory, Kirk Road and Pine Street, Batavia, Il 60510, USA

J. Estrada
e-mail: estrada@fnal.gov

G. Cancelo
e-mail: cancelo@fnal.gov

H. T. Diehl
e-mail: diehl@fnal.gov

G. Fernández Moroni
Comisión de Investigaciones Científicas y Técnicas (CONICET), Buenos Aires, Argentina

S. E. Holland
Lawrence Berkeley National Laboratory, 1 Cyclotron Road, Berkeley, CA 94729, USA
e-mail: seholland@lbl.gov

E. E. Paolini
Comisión de Investigaciones Científicas Prov. Buenos Aires (CIC), Buenos Aires, Argentina

Published online: 06 May 2012

advantages for low noise applications are discussed. A technique for obtaining sub-electron readout noise levels is presented, and its noise and signal characteristics are derived. We demonstrate that with this procedure a very low readout noise of $0.2e^-$ RMS can be achieved. The contribution of other noise sources (output stage, vertical and horizontal charge transfer inefficiency, and dark current noise) are also considered. The optimum number of samples for achieving the total lowest possible noise level is obtained. This technique is applied to an X-rays experiment using a ^{55}Fe source.

Keywords Skipper CCD · Sub-electron noise · Floating gate output stage

1 Introduction

Since its invention as a memory device, CCDs have been widely used as imaging detectors because of their capability to obtain high resolution digital images of objects placed in its line of sight. Astronomy and spectroscopy applications have been using this technology since its invention [1, 2] encouraging continuous improvements [3, 4]. Nowadays, scientific CCDs are developed with high performance characteristics for visible and infrared light detection, with quantum efficiencies above 90%, wide dynamic range with capability to handle signals producing more than 100,000 e^- RMS, and pixel size around 10 μm [5]. However the readout noise (RN) caused by the CCD output stage is still the main limitation when these detectors are used for low signal detection or energy discrimination of slightly different signals.

The RN is an error in the pixel value caused by electrical noise added to the CCD video signal. The main source of this electronic noise is the CCD output amplifier but the readout system and the bias and clocks signals used for charge collection and transfer do also contribute [4, 5]. The readout system is in charge of recovering and digitizing the pixel value encoded as the difference between two constant levels in the video signal, therefore electronic noise fluctuations altering those levels are interpreted as variations in the collected charge.

In this paper a scientific CCD fabricated on a high-resistivity silicon substrate with the capability of multiple sampling of the charge signal, known as Skipper CCD is described [6, 7]. Its architecture and its advantages for low noise applications are discussed. A technique for obtaining sub-electron readout noise levels is presented, and its noise and signal characteristics are derived. We demonstrate that a very low readout noise of $0.2e^-$ RMS can be achieved. The contribution of other noise sources (output stage, vertical and horizontal charge transfer inefficiency, and dark current noise) are also considered. The optimum number of samples for achieving the total lowest possible noise level is obtained.

The paper is organized as follows. In Section 2, a brief description of the Skipper CCD is provided, and its output stage is compared with the floating diffusion output stage commonly used for standard CCDs. The capability of non-destructive, multiple reading of the same pixel is also described. The

typical sources of video signal noise are described in Section 3, and the readout systems of standard and Skipper CCDs are reviewed. Their frequency responses are derived, and the Skipper noise reduction capabilities are analyzed. Some experimental results, including the effect of dark current noise and charge transfer inefficiency are described in Section 4. Also some hints on selecting the parameters of the readout system are given. Finally, some concluding remarks are provided in Section 5.

2 Skipper CCD detector

This detector (Fig. 1) was developed at Lawrence Berkeley National Laboratory in 2010. It is a *p*-channel front illuminated CCD fabricated on high-resistivity, *n*-type silicon. A low density impurity doping in the *n*-region together with a reverse bias voltage in a ohmic contact in the wafer back side allows to operate the detector with a large fully depleted region increasing the quantum efficiency for infrared light. The resistivity is about 4 k$\Omega \cdot$ cm to 5 k$\Omega \cdot$ cm and 40 V is a common substrate voltage for the detector. Using this combination, it is possible to obtain a depletion region width of around 250 μm in comparison with the 10 μm to 20 μm of standard detectors [8]. A cross section of the CCD for one pixel is shown in Fig. 2.

The detector is arranged as 1022 by 1024 square pixels with a pixel width of 15 μm. The sensors are grouped in four regions (L1, L2, U1 and U2) which are read by four amplifiers placed in each corner of the chip. The horizontal registers that move the charge to the output stage are placed in two sides of the detector (Fig. 3). Both horizontal and vertical gates are arranged in a three phase configuration [5] where V1, V2 and V3 move the charge vertically, and

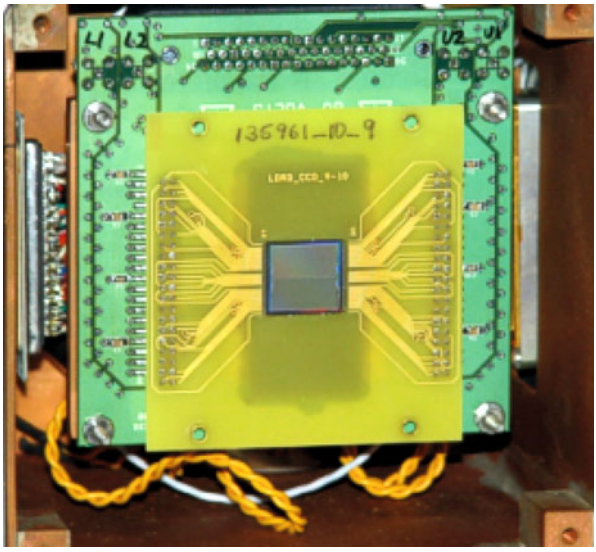

Fig. 1 Skipper CCD in a testing package mounted in a dewar at Fermilab

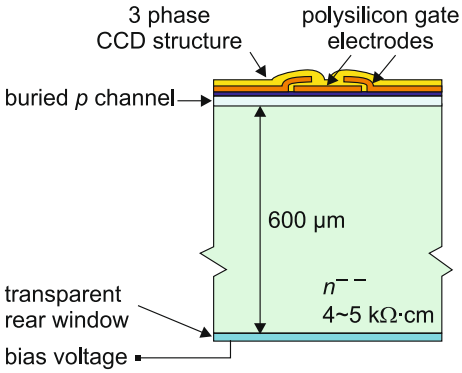

Fig. 2 Cross section of a pixel in the Skipper CCD (from [8])

H1, H2 and H3 transfer it horizontally to the output amplifier. In the output stage the charge is moved by the summing well gate (SG), output gate (OG) and dump gate (DG) clocks (see Section 2.1).

The charge packet is transferred to the sense node, where the output amplifier in common source configuration drives the video signal to the readout system. A distinctive feature of the Skipper CCD is its floating gate output stage [6, 9] that allows for non destructive charge measurements, instead of the common floating diffusion output stage used in standard CCDs. The layout of the output stage of the L2 amplifier is shown in Fig. 4, where the floating gate, the output gate and the summing well gate are detailed.

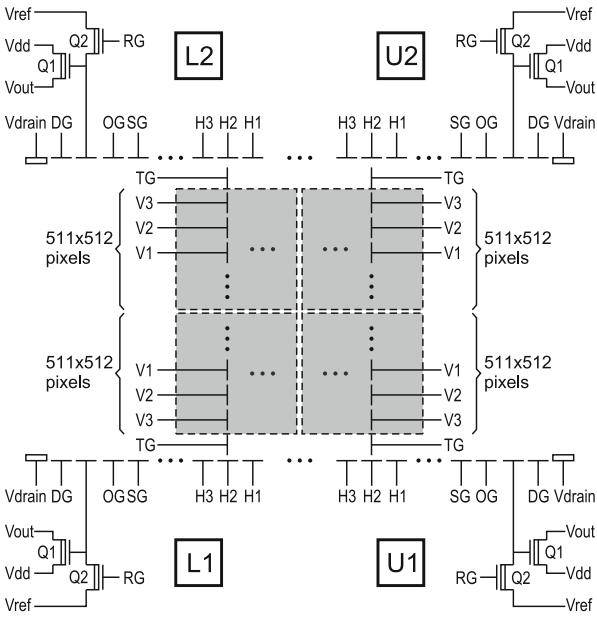

Fig. 3 Skipper CCD Architecture. Each of the four amplifiers (U2, U1, L1 and L2) handles a 511 by 512 pixel region

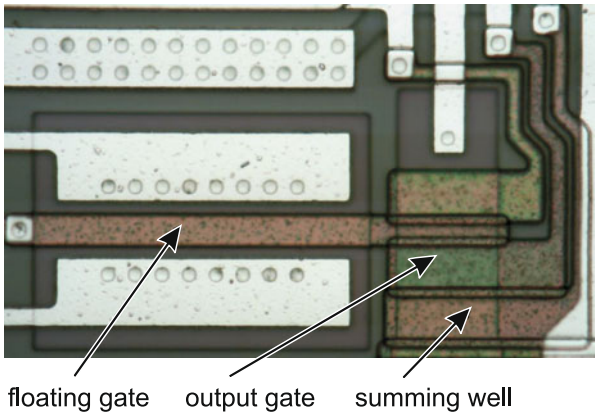

Fig. 4 L2 amplifier layout. The floating gate, the output gate and the summing well gate are shown

2.1 Skipper operation

The main advantage of the floating gate output stage of the Skipper CCD is its capability of performing multiple pixel readings with minimum effect on the stored charge. The flow of the charge is controlled by the summing well gate (SG), output gate (OG) and dump gate (DG) clock, and the timing of these signals for reading out the same pixel three times are shown in Fig. 5. In t_0 the charge package is placed under the last H3 gate at the end of the serial register. The SG clock goes down attracting the charge pocket under its gate. After a few microseconds H3 goes high and the charge remains completely stored under SG. At the same time DG and the reset gate (RG) signals go down to remove the previous pixel charge from the channel and to set the new reference voltage for the current pixel. In t_1 the charge is transferred from the SG to the sense node through the OG. The SG is set high increasing its channel potential above the OG barrier so the charge moves to the potential well set by the last reset pulse in the sense node. At this point the charge produces a change in the reference level at the output transistor gate that is reflected as a step increment in the output video signal (V_{video}). The skipper cycle continues when the holes are transferred backwards to the SG in t_2. This process is achieved by setting OG and SG to a low level. Because the SG sets a lower channel potential all the charge moves under its surface and the OG acts like a potential barrier to confine the charge (in this case, under the SG). In t_3, after the charge is moved out from the sense node, the RG resets the floating gate to the V_{ref} voltage resulting in a new reference level for the new pixel sample. The pixel value is encoded as the difference of two constant levels. The reference level is called the *pedestal level*, and the second one the *signal level*.

By repeating t_1, t_2 and t_3 cyclically, several measurements of the same pixel can be performed. After reading the desired number of samples, the pixel reading procedure is completed when the charge is removed from the channel and the floating gate is reset by the DG and RG pulse in t_0 (of the next pixel),

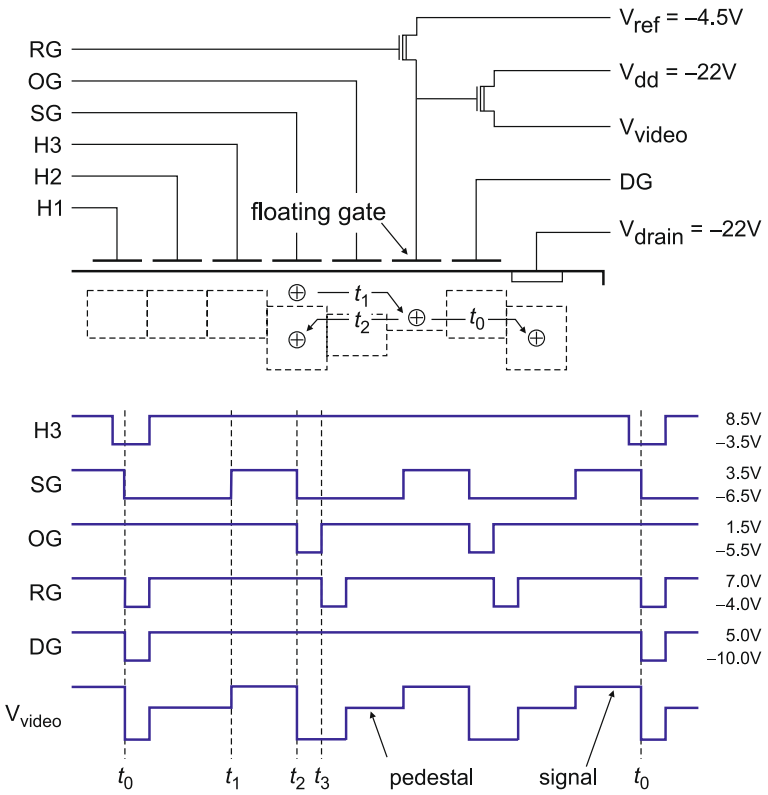

Fig. 5 Skipper output stage and timing

respectively. When DG goes down, it leaves a potential path between the sense node and the V_{drain} ohmic contact for channel discharging.

2.2 Sensitivity of the output stage

The floating gate output stage of Skipper CCD differs from the traditional floating difussion output stage used in typical CCDs because other capacities load the charge transport channel. Its effects on the sensitivity (voltage increment at the CCD output per hole collected) and a comparison with the sensitivity of the standard floating diffusion output stage are analyzed in this section.

2.2.1 Floating diffusion output stage

Floating diffusion is the typical output stage configuration in standard CCDs. It provides the highest sensitivity because the output amplifier gate is connected directly to the CCD channel providing a minimum capacitance load. When a

package of charge ΔQ is transferred to the floating diffusion node, it produces a voltage

$$\Delta V = \frac{\Delta Q}{C_J + C_{\mathrm{PFD}} + C_{\mathrm{IN}}}, \tag{1}$$

where $C = C_J + C_{\mathrm{PFD}} + C_{\mathrm{IN}}$ is the total capacitance between the node and ground composed by the junction capacitance between the floating diffusion and the bulk (C_J), the parasitic capacitance at the node (C_{PFD}), and the capacitance of the output amplifier (C_{IN}) that includes contributions from both the source follower and reset transistors. The input-referred noise of the output stage depends directly on C [5], and therefore it should be minimized to achieve a low-noise output stage.

2.2.2 Floating gate output stage

In the floating gate configuration of the output stage of the Skipper CCD, the gate of the output transistor is connected to a gate electrode placed over the channel where charge is transported, as depicted in Fig. 4. The signal charge induces a potential change on the floating gate electrode that is sensed by the output transistor. The change in voltage at the floating gate for a given amount of signal charge ΔQ is given by [9, 10]

$$\Delta V = \frac{\Delta Q}{C_{\mathrm{PFG}} + C_{\mathrm{IN}} + (C_{\mathrm{PFG}} + C_{\mathrm{IN}} + C_{\mathrm{OX}})C_{\mathrm{B}}/C_{\mathrm{OX}}}, \tag{2}$$

where C_{OX} is the capacitance between the floating gate and the channel, C_{B} is the capacitance between the channel, bulk and channel stop regions, and C_{PFG} is the capacitance between the floating gate, channel stops and adjacent output and dump gates, caused by the overlap of the polysilicon gate electrodes as seen in Fig. 4. For CCDs fabricated on high-resistivity silicon, the capacitance between the channel and bulk is very small because of the large depletion region. In addition, the capacitance between the channel and channel stop is small compared to C_{OX} because the wide depleted region between the signal charge and channel stop is much larger than the insulator thickness between the channel and the floating diffusion. Therefore $C_{\mathrm{OX}} \gg C_{\mathrm{B}}$ for the CCDs considered here, and the sensitivity for the floating gate is mainly determined by C_{PFG} and C_{IN}.

In the Skipper CCD prototype tested, each of four CCD regions have floating electrode gates of different areas and widths for each amplifier to analyze the effects of the floating electrode geometry on the sensor performance (L1: 216 μm^2, L2: 96 μm^2, U1: 60 μm^2, U2: 96 μm^2). To date, only one floating-gate configuration out of the four designs has been studied in detail. It has a sensitivity (charge-to-voltage conversion gain) of 3.5 μV/e^- [8], similar to the sensitivity of the Dark Energy Survey (DES) CCDs with floating diffusion outputs [11].

3 Output amplifier noise and readout systems

Regardless of the type of CCD output stage, the pixel measurement is differentially encoded between two constant levels in the video signal, and the amount of charge can be computed simply by their subtraction. However, the signal is corrupted by electronic noise originated mainly in the output transistor, and more sophisticated readout methods are required to achieve low RN. There are two different mechanisms that produce signal fluctuation, and each one is characterized by a distinctive power spectrum density (PSD) with different RN contribution to the pixel value. These noise sources are [5, 6, 12, 13]:

- white thermal and shot noise, caused by random fluctuation of free charges that are part of the transistor current;
- low frequency (LF) noise, caused by two accepted mechanisms: traps in the output transistor Si-SiO_2 surface and bulk region that catch and release moving charge for relatively long periods, and mobility fluctuations by phonons in the channel. Both produce a noise with a PSD that varies inversely with frequency.

An accepted model for MOSFET noise PSD is [5]

$$S_n(f) = \sigma_0^2(1 + (f_c/f)^m) \tag{3}$$

where the σ_0^2 is the white noise PSD which is flat for all frequencies, f_c is the corner frequency at which both LF and white noise PSDs take the same value, and m is an exponent that usually takes values between 1 and 2 [5]; depletion mode FETs exhibit LF noise PSD with exponents greater than 1 caused by interface and Si bulk traps that have a Lorentzian spectrum [12, 13]. This exponent can also be temperature dependent because of the activation of different energy traps at different temperatures [12, 13].

As an example, Fig. 6 shows the noise PSD for a depletion MOSFET fabricated on high resistivity silicon. Not only the temperature dependency is clearly depicted, but also the rate of inverse variation of the PSD with the frequency. While the PSD has a slope proportional to $1/f^2$ for a temperature of 293 K, it changes to a $1/f$ proportionality for a temperature of 133 K. The corner frequency also changes with the temperature.

Each noise mechanism produces different effects in the pixel error at the output image. While white noise has a mayor impact for high speed readings, the LF noise sets the minimum reachable pixel error at slow readout operation.

3.1 Readout system

The main task of the readout system is to recover the pixel value while minimizing errors due to electronic noise. A widely used readout system is the Dual Slope Integrator (DSI) [5] because it provides an optimal filtering for white noise [4] and completely rejects the reset noise. Instead of taking just one sample of each constant level, the DSI performs the difference of the result

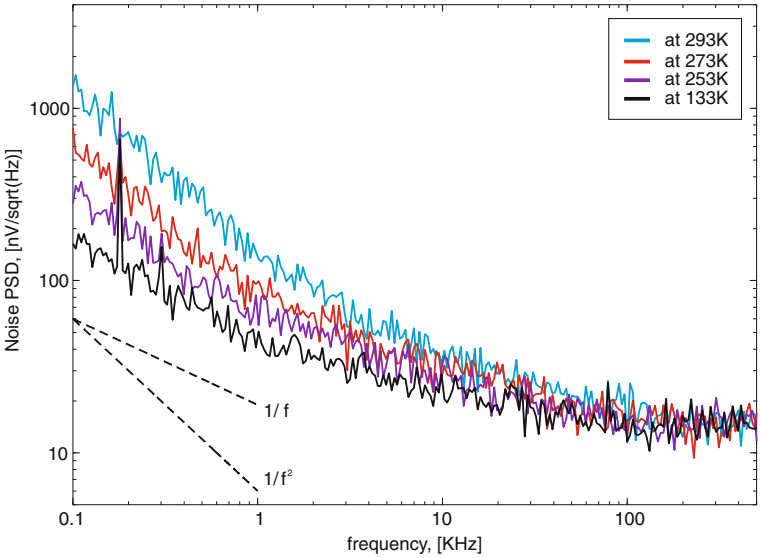

Fig. 6 CCD output amplifier noise for a depletion MOSFET fabricated on high resistivity silicon. The noise PSD is plotted for different temperatures. Reference slopes for $1/f$ and $1/f^2$ are also depicted

of integrating during a given time interval the pedestal and the signal levels. In the Skipper CCD, each of the multiple measurements for each pixel is performed by a DSI system. In what follows, the spectral characteristic of the DSI and Skipper CCD readout are obtained, and its influence on the readout performance is analyzed.

3.1.1 DSI readout system

The frequency response of the DSI readout system can be derived from its impulse response. The pixel value is the difference between the results of the pedestal and signal level integrations, and therefore the DSI impulse response is given by

$$h_{DSI}(t) = \begin{cases} A/T_S, & t_0 \le t \le t_0 + T_S, \\ -A/T_S, & t_0 + T_S \le t \le t_0 + 2T_S, \\ 0, & \text{otherwise}, \end{cases} \tag{4}$$

where A is an arbitrary integration gain, t_0 is an arbitrary time instant when the pedestal begins, and T_S is the integration time of both the signal and pedestal levels; the total integration time is $T_T = 2 \times T_S$. This model assumes that transients in the video signal from the CCD that occur in the transition between pedestal and signal intervals, and vice versa, and others caused by

clock leakages, etc. have been removed. From now on, we consider $t_0 = 0$ for simplicity. The module of the frequency response is the Fourier transform of (4)

$$|H_{DSI}(f)| = \frac{2A}{\pi T_S f} \sin^2(\pi T_S f). \tag{5}$$

Plots of $|H_{DSI}(f)|$ for two different integration times are shown in Fig. 7. The frequency response for $T_S = 55\ \mu$s is plotted as a black dashed curve (a), and for $T_S = 5.5\ \mu$s as a black solid trace (b). When the total integration time T_T is increased, the frequency response curve shifts to a lower frequency band, and its bandwidth decreases, (each lobe gets thinner) reducing the effective bandwidth of the readout system. Therefore, the incidence of white noise on the pixel value is reduced. However, this RN reduction is limited by the LF noise, because the frequency response curve shifts to lower frequencies where the noise PSD is higher. In fact, the maximum point of the FR is allocated approximately at $f_{\max} \approx 0.37/T_S$ which is inversely proportional to the readout time.

The contribution of white noise and LF noise can be computed from the noise model of (3) and the frequency response given by (5) as a function of the integration time:

– white noise: the pixel error variance is reduced by the inverse of the integration time ($\propto 1/T_S$),

$$\sigma_w^2 = \frac{2}{T_S}\sigma_0^2, \tag{6}$$

where σ_0^2 is the white noise PSD.

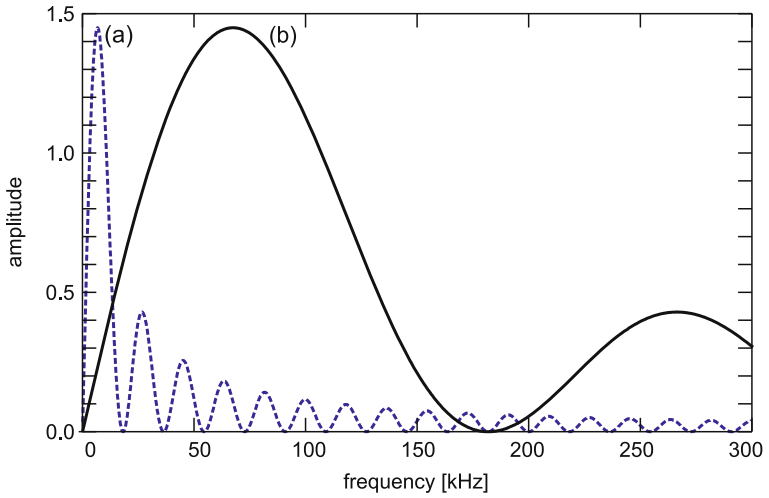

Fig. 7 Frequency response of the DSI readout system for $T_S = 55\ \mu$s (**a**) and $T_S = 5.5\ \mu$s (**b**)

– LF noise: the error variance is proportional to T_S^{m-1}, where m, $1 \leq m \leq 2$, is the exponent of the noise PSD in (3),

$$\sigma_{\mathrm{LF}}^2 = 16 \cdot 2^{m-1}(1 - 2^{m-1})\Gamma(-m-1)\sin(\pi m/2)\sigma_0^2 f_c^m (\pi T_S)^{m-1}, \tag{7}$$

where $\Gamma(\cdot)$ is the Gamma function, $\Gamma(z) = \int_0^\infty t^{z-1}e^{-t}$.

These relations show that the white noise contribution can always be reduced by increasing the integration time T_S, but the LF cannot. In fact, if the PSD does not have a slope $m = 1$ its contribution slowly increases for longer integration times. Therefore exists an optimal integration time T_S that simultaneously minimizes the effects of both white noise and LF noise. This behaviour has been measured for many CCDs used for DECam project [14]. The minimum noise level achieved by this technique in detectors with floating diffusion output stage is around $2e^-$ RMS [5, 8, 14].

3.1.2 Skipper CCD readout system

The multiple readout technique allows to reduce the RN below the $2e^-$ RMS limit of state-of-the-art DSI systems to achieve sub-electron RN. In the Skipper CCD the readout system averages N samples for each pixel to get its final value, and each sample is read using the DSI technique. The impulse response $h_{SKP}(t)$ of the readout system is a linear combination of time shifted copies of $h_{DSI}(t)$:

$$h_{SKP}(t) = \frac{1}{N}\sum_{n=0}^{N-1} h_{DSI}\left(t - n(\tau + T_S)\right), \tag{8}$$

with

$$h_{DSI}(t) = \begin{cases} A/T_S, & t_0 + \tau \leq t \leq t_0 + \tau + T_S, \\ -A/T_S, & t_0 + \tau + T_S \leq t \leq t_0 + \tau + 2T_S, \\ 0, & \text{otherwise}, \end{cases} \tag{9}$$

where τ is the time interval between samples and T_S is the integration time for one sample. In this case each pixel is read N times employing a total integration time of $T_T = 2 \times N \times T_S$.

Using Fourier transform properties, and assuming $t_0 = \tau = 0$ for simplicity, the module of the frequency response for the skipper readout system can be computed as

$$|H_{SKP}(f)| = \frac{2A}{\pi N T_S f}\sin^2(\pi T_S f)\left|\frac{\sin(\pi N T_S f)}{\sin(\pi T_S f)}\right|. \tag{10}$$

The performance of the Skipper CCD readout system can be explained with the help of Fig. 8. Curves (a)–(d) depict the frequency response of the readout system for different values of T_S and N. Curves (b), (c) and (d) correspond to the same sample time $T_S = 2.5\ \mu$s but increasing number of averaged samples

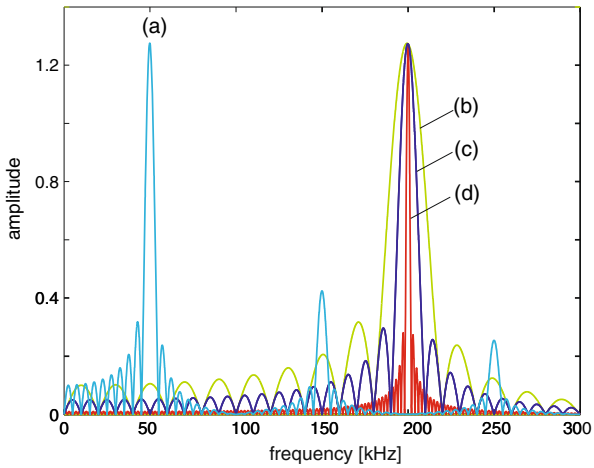

Fig. 8 Frequency response of the Skipper readout system for $T_S = 10\ \mu$s and $N = 10$ (**a**) and for $T_S = 2.5\ \mu$s and $N = 10$ (**b**), $N = 20$ (**c**) and $N = 100$ (**d**)

$N = 10, 20, 100$, respectively. As T_S remains constant and only N is augmented the main lobe of the responses remains fixed at same frequency, in this case centered approximately at 200 kHz. At the same time, the width of the lobes is reduced according to $1/N$, and the secondary lobes reduce their amplitudes. Therefore, an effective reduction of the gain at low frequency is obtained, and white and LF noise effects are reduced simultaneously.

To analyze the effect of increasing T_S, the curve (a) corresponding to $T_S = 10\ \mu$s and $N = 10$, is compared to curve (b) which uses the same N but a smaller T_S, $T_S = 2.5\ \mu$s. As T_S is increased the main lobe displaces to lower frequencies increasing the system gain in this region. The effect of white noise is reduced because the lobe width is proportional to $1/T_S$ and the effective bandwidth is reduced. However, no improvement is obtained on the LF noise reduction, as explained in the previous section for the DSI system.

A quantitative analysis of the reduction for each noise type is possible using (3) and (10); however it is not possible in this case to obtain closed-form expressions as in (6) or (7) for the DSI system.

The white noise effect can be reduced increasing either N or T_S because it depends on the total integration time $T_T = 2NT_S$. The RMS value of the pixel error is reduced according to $1/\sqrt{NT_S}$.

The LF noise effect can be only reduced increasing the number of samples N. It was found that the RMS value of the pixel error depends on the exponent m of the LF noise PSD:

- for $m = 2$ the RMS pixel error decreases with $1/\sqrt{N}$.
- for $1 \leq m < 2$, further reduction is obtained increasing N for decreasing values of m, following a relationship $1/N^{\alpha}$ with $0.5 < \alpha < 0.6$.

These results suggest a procedure for selecting the parameters of the Skipper CCD readout system: (1) choose the largest sample time T_S to provide white noise filtering, while avoiding the domination of LF noise effect over

the pixel error; and (2) increase the total integration time by augmenting the number of samples N, reducing both the LF and white noise pixel errors simultaneously. Clearly, the additional RN reduction comes at the expense of an increased readout time.

Although in theory there is no limitation in RN reduction by increasing the number N of averaged samples, there is a practical limit imposed by some losses in the charge transfer, and other on-chip noise sources that could become significant limiting the CCD performance, particularly the dark current noise. Further elaboration is provided in Section 4.

Therefore, choosing appropriate values for the sample time T_S and the number of averaged samples N, the Skipper CCD readout system can be adjusted to reduce LF and white noise effects allowing a RN level below the $2e^-$ RMS LF noise floor achieved commonly in scientific CCDs.

3.2 Comparison of DSI and Skipper performance

The main advantage of the Skipper readout system is revealed when its frequency response is compared to the standard DSI frequency response for the same total integration time, i.e., using the same total amount of time for reading each pixel. In Fig. 9 the frequency response $|H_{DSI}(f)|$ of the DSI readout system (curve (b)) is plotted for $T_T = 110\ \mu$s, together with the frequency response of the Skipper readout system for $T_S = 5.5\ \mu$s and $N = 10$ (curve (c)), using a logarithmic frequency axis. The noise PSD from Fig. 6 for a temperature of 273 K is also included (curve (a)). Both systems achieve the same level of white noise reduction because the total integration time T_T of the video signal is the same in both cases. However, the gain of Skipper CCD readout system is much lower than DSI readout system at low frequencies, allowing a RN reduction in presence of LF noise. This reduction can be increased by merely augmenting the number N of averaged samples. In other words, low frequency noise filtering is achieved and the LF limitation is removed, at the only expense of increasing readout time.

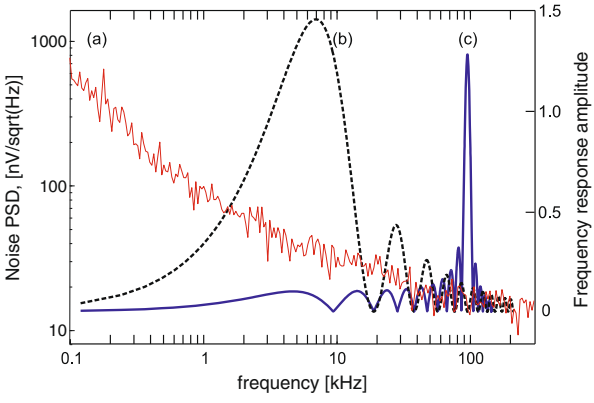

Fig. 9 *Left axis* Depletion MOSFET noise PSD at a temperature of 273 K (**a**). *Right axis* frequency response of DSI readout system for $T_T = 110\ \mu$s (**b**) and of the Skipper readout system for $T_S = 5.5\ \mu$s and $N = 10$ (**c**)

4 Experimental results

In this section the performance of the skipper CCD is addressed by way of experimental measurements. First, the readout noise reduction is studied and tested for pixels in the overscan region of the CCD, obtaining very deep sub-electron RN (0.2 e^- RMS). Second, the behavior of the CCD when subject to a ^{55}Fe X-Ray source is analyzed, and the charge transfer capacity of the output stage is determined. Finally, the contribution of other CCD on-chip noise sources are studied to determine the optimum operating point of the detector.

The readout system utilized in these experiments was originally developed for the DECAM project (Dark Energy Camera, [11]) at Fermilab [15, 16], that was modified to handle the skipper technology. The CCD, placed in an aluminium dewar and run at 143 °K to diminish dark current generation, was tested at one of the Fermilab's laboratories.

The readout noise for a single pixel sample was somewhat higher that expected form measurements on similar sensitivity CCDs [8], as explained in Section 2.2.2. It is expected to develop in the near future a new readout electronics with lower noise level specifically tailored to the Skipper CCD that could improve the results presented in this article.

For the multiple sampling of the Skipper CCD the final images were obtained off-line by averaging the samples corresponding to the same pixel by software. The calibration of the system for different experiments was performed using an X-ray ^{55}Fe source. In every case, the gain of the system was determined from the final averaged images.

4.1 Readout noise measurements

As stated in Section 3.1.2, the RN level can be reduced by increasing the number N of samples read from each pixel. To analyze the actual performance of the mutiple-sampling capability of the Skipper CCD a series of measurements in the detector's overscan region were performed. These pixels are not affected by other noise sources such as charge transfer inefficiency nor dark current generation because they are free of charge; the only noise contribution is additive electronic noise from the output amplifier and the readout system. As a result the reduction rate of the RN when increasing the number of samples N can be obtained. The results corroborate that the reduction rate depends on the dependency of the PSD of the LF noise with the frequency. For the Skipper CCD it is possible to find the number of samples N required for obtaining sub-electron RN level. It is shown that under these conditions, very deep sub-electron RN can be achieved.

Previous experiments have shown that the lowest RN for one-sample lecture was achieved with a sample time of 10.4 μs, and therefore this value was chosen to perform multiple pixel sampling, according to the procedure outlined in Section 3.1.2. For this integration time the system gain is 0.06 e^-/DN that results in a negligible quantization noise of 0.017 e^- RMS. Figure 10 shows

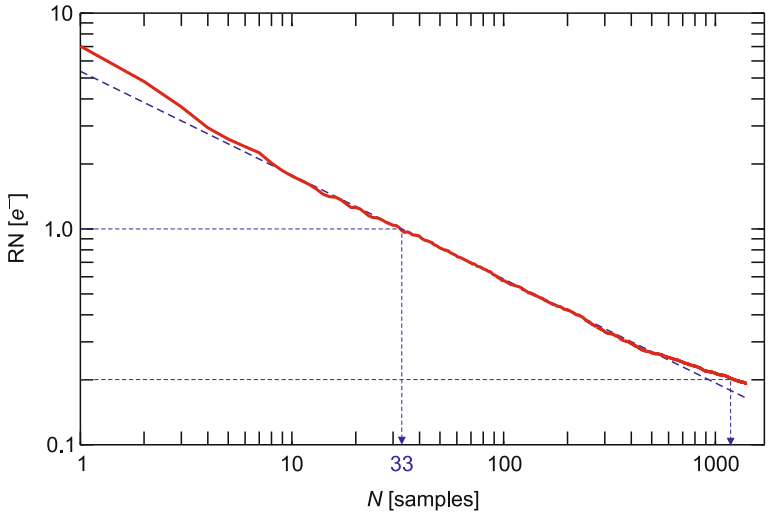

Fig. 10 Skipper CCD RN in the overscan region as a function of the number of averaged samples N. *Continuous line* RN measured from images. *Dashed line* theoretical RN reduction fit for white or $1/f^2$ noise

the RN in electrons (e^- RMS) measured from the images as a function of the number N of samples averaged for each pixel (continuous line). The dashed line has a slope proportional to $1/\sqrt{N}$ that shows the RN reduction that should be expected if the only noise sources were white noise and $1/f^2$ noise. Three regions are clearly distinguishable, according to the number of samples N:

- For low number of averaged samples (up to approximately $N < 10$) the measured curve deviates from the straight line, revealing faster decreasing of RN, proportional to $1/N^{0.6}$. This suggests that the mayor contribution of the RN in this range is produced by LF noise which has a PSD with a tendency close to $1/f$.
- For N between 10 up to 500 the RN noise closely follows the $1/\sqrt{N}$ profile, suggesting that either white noise or $1/f^2$ noise dominates the effects in the RN.
- For larger values of the number of averaged samples ($N > 500$) the RN decreases more slowly, suggesting the contribution of LF noise whose PSD decreases faster than $1/f^2$, or of other unidentified noise sources. This noise sources may have origin in the readout electronics.

The figure reveals that sub-electron RN can be obtained for $N = 33$ and a RN $= 0.2e^-$ RMS is achieved when averaging $N = 1227$ samples. This gives a total pixel readout time of 686 μs and 25 ms, respectively. The same results are depicted in a more intuitive form using histograms in Fig. 11. The width of the Gaussian distribution is greatly reduced by the averaging of samples, and for $N = 200$ all the RN values are practically contained within the $2e^-$ RMS segment, allowing for very low signal detection.

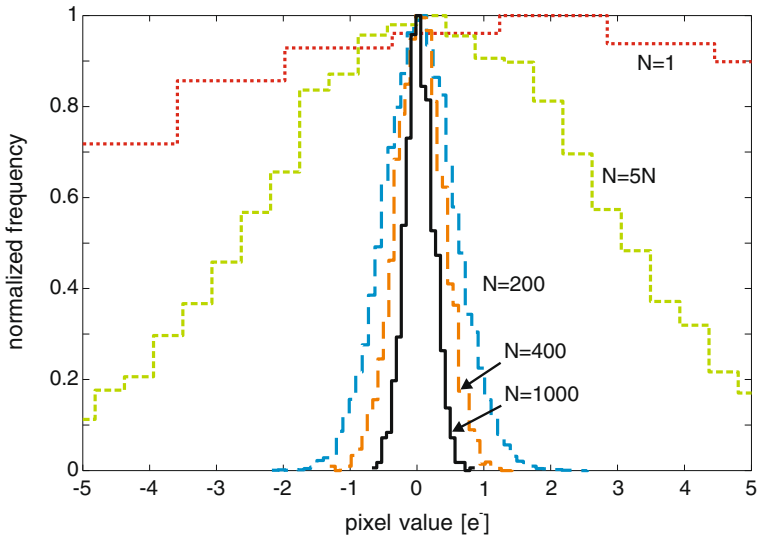

Fig. 11 Sample histogram of the background pixels from the final images of the Skipper CCD for different numbers of averaged samples per pixel N. The histograms are normalized to their maximum values and the pixel value is in electrons

4.2 ^{55}Fe X-rays

In this section, the performance of the detector and the charge transfer capacity of the output stage of the Skipper CCD are analyzed.

Images were taken by continuously reading the detector while it was exposed to a ^{55}Fe X-Ray source. In order to not slow the reading, and to avoid high X-ray density in every image, only a portion of the detector (600 rows by 5 columns) was scanned using multiple sampling mode with 200 samples per pixel. The rest of the image was read taking only a sample per pixel. This lecture mode is represented in Fig. 12. The central portion of the figure corresponds to the multiple reading of the 5 columns by 600 rows pixels. Each measurement was arranged on the same line, one next to the other, so that every line in each of these five columns represents the 200 readings. The X-ray measurements are represented by the white lines in this region. To the left and to the right of the multiple sampling zone, some X-rays events read with one sample per pixel can also be seen. To avoid fixed pattern noise, a bias image obtained by averaging 15 images not exposed to the source was subtracted from the output images before performing noise and X-ray analysis.

The sample time was $T_S = 5.5\ \mu$s, and the total integration time in the multiple sampling region of the Skipper CCD was $T_T = 2.2$ms. The readout system gain for this integration time is 0.12 e^-/DN, and the quantization noise (merely 0.035 e^- RMS) does not have major impact on the measurements.

The RN for one sample is 10.8 e^- RMS which is somewhat larger than expected (see comments above). The variation of the RN in RMS electrons

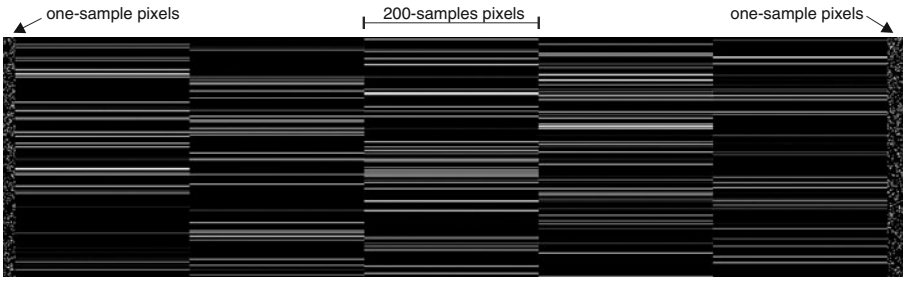

Fig. 12 A portion of the Skipper output image. White traces correspond to 200 samples of the same pixel with X-rays events. Five columns of the CCD were read in multiple sampling mode operation. Some events corresponding to 1 sample per pixel are seen at both sides of the image

as a function of the number of averaged samples in the active region is shown in Fig. 13. This figure reveals that the RN can be reduced to 0.73 e^- RMS after averaging $N = 200$ samples. The measured RN behaves as expected from the analysis in Section 3.1.2 and similar to the measurements of the overscan region analyzed in Section 4.1.

A sample of the ^{55}Fe spectrum obtained after multiple sampling is shown in Fig. 14. This spectrum was obtained by considering only single pixel events. The measured width of the ^{55}Fe K_α line is 151 eV (FWHM) which is in a good agreement with predictions of 135 eV and 142 eV of reported measurements of CCD Fano factors in [17] and [18, 19], respectively. For comparison purposes, using data obtained in single sample readout region the width of the K_α peak FWHM is 199 eV. These values show the improvement in energy resolution and better discrimination of single pixel events that can be achieved by multiple sampling because of the reduced readout noise. However, it must be taken into account that this experiment was not planned for high resolution energy measurement, but only to test Skipper CCD capabilities for low noise measurement. More accurate experiments are required to achieve statistically sound results.

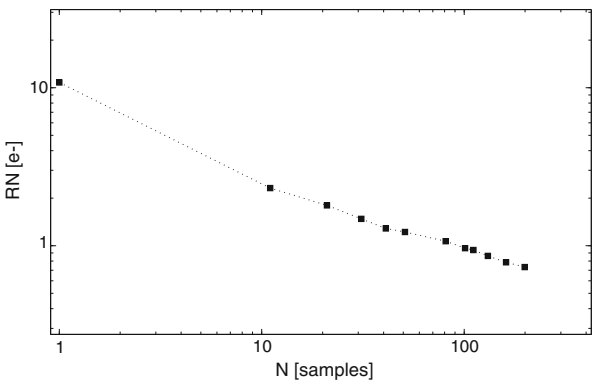

Fig. 13 Skipper CCD RN as a function of the number of averaged samples N in the active region

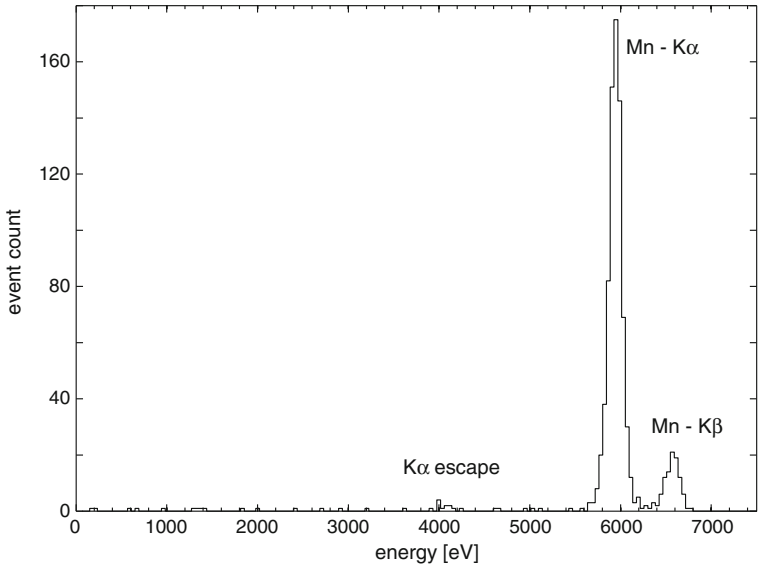

Fig. 14 ^{55}Fe X-ray source spectrum using the Skipper CCD in multiple sampling mode

The K_α peak in Fig. 14 also shows a Gaussian profile and no low energy tail, suggesting a good charge transfer at the output stage. In order to address this effect the charge transfer inefficiency (CTI) was measured for the pixels with charge packets corresponding to the K_α peak. For each pixel in the multiple sampling region the charge value for each of the 200 samples vs the sampling number was approximated by a linear least square fit. The normalized slope of the fitted model is the CTI, and its value for each pixel comprised in the multiple-sampling region is shown in Fig. 15. The dispersion of the CTI values is in agreement with the theoretical error of 8×10^{-6} RMS expected from the RN measurements. The mean CTI value of 1.8×10^{-6} is plotted as a horizontal line in the figure.

Because the final pixel value is the average of all the samples, the average CTI is twice the actual CTI of the output stage. Therefore, the CTI of the detector is 0.9×10^{-6}. This means that 0.00009% of the charge is lost in the back-and-forth transfer of the multiple reading mode of the Skipper CCD, demonstrating the good charge transfer at the output stage.

4.3 General noise analysis

The purpose of achieving the lowest noise level in the detector is to allow the detection of very weak signals, depositing a few electrons per pixel. The capacity of the Skipper CCD to achieve sub-electron noise levels have been addressed in previous sections. This section elaborates on the performance obtainable when all the pixels in the detector are read. At these noise levels other on-chip sources of perturbation become significant and should be also

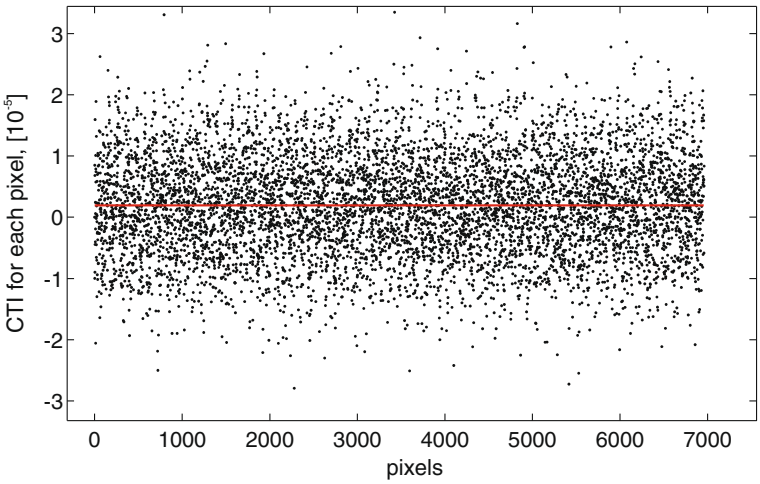

Fig. 15 Measured output stage CTI for pixels in the multiple sampling region with charge packet corresponding to X-rays in the K_α peak of the ^{55}Fe source spectrum

considered. The mayor sources are output stage charge transfer inefficiency, vertical and horizontal charge transfer inefficiency, and dark current.

Output stage charge transfer analysis was addressed in the last subsection, and a CTI of 0.00009% was found. This suggest that pixels with a few electrons charge can be sampled nearly 1000 times without significant charge degradation.

Another mechanism for charge loss to be considered is the horizontal and vertical transfer of charges in the array. The vertical and horizontal charge transfer inefficiency measured for several detectors fabricated on high resistivity silicon was found to be less than 1×10^{-6} [15]. The pixel in the last row and column in the array is the one that experiment the major charge loss; other pixels in the array are less affected because less transfers are needed to displace its charge to the output stage. In the Skipper CCD the charge of this pixel has to be transferred 512 rows and 511 columns, losing an average of 0.001 of its charge to arrive at the output stage. This degradation is very low, and does not affect the detection of very weak signals.

Dark current (DC) is another important source of degradation of energy resolution and it imposes a limit in the maximum number of samples. DC noise is time dependent and can affect the performance of the detector for large readout times, or in the case of Skipper CCD when a high number of samples N are averaged to obtain very low RN. Figure 16 shows the dark current generation (average number of generated charge per pixel per hour) as a function of the temperature, measured for a CCD fabricated on high resistivity silicon at Fermilab's labs [15]. For similar CCDs running at 100 K for the DAMIC experiment [20], a DC of 2 electrons per pixel per day was measured. These measurements are particularly difficult because it is difficult to discriminate

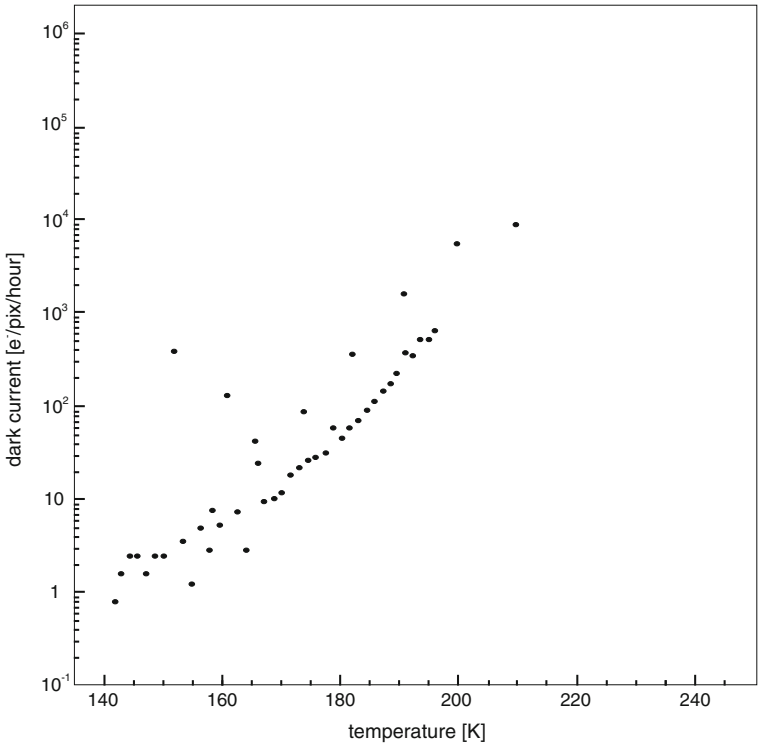

Fig. 16 Dark current measurements for a CCD fabricated on high resistivity silicon [15]

the leakage current generation from environmental radiation at those low background levels.

For the ^{55}Fe-experiment in last section, the readout time for each image was approximately 18 s. The detector was run at 143 K, and according to Fig. 16, an average DC generation of 1 e^-/pixel/hour is expected, or 0.005 e^- after 18 s. Assuming that the charge generation due to DC follows a Poisson distribution, the added noise is about 0.07 e^- RMS, that is an order of magnitude lower than the background RMS noise value measured in the images. Although in this case the noise attributed to DC generation is very low, this figure increases when all the detector is read in the multiple-sampling mode (in the experiences of Section 4.2, only an area of 600 × 5 pixels was read in this mode). In this case, the reading time can take several minutes making the DC contribution to noise significative, and even limit the system performance. Therefore, the RN and DC noise generation must be considered simultaneously to achieve the lowest possible noise level on the detector.

In the case of the Skipper CCD, the DC generation limits the number of samplings N of each pixel. The RN (RMS) as a function of N can be approximated from the fitted curve in Fig. 10 as

$$\sigma_{RN} = \sigma_1/\sqrt{N},$$

where σ_1 is the RN for $N = 1$ and for a given T_S. Assuming that the Skipper CCD is read continuously, the dark current noise (RMS) can be modelled as

$$\sigma_{DC} = (2 \times 511 \times 512 D_C N T_S)^{1/2},$$

where D_C is the average dark current generation at the operating temperature. The total noise is the sum in quadrature of both contributions, and its minimum value is obtained when

$$N = \frac{0.0014\sigma_1}{\sqrt{D_C T_S}}.$$

Assuming $T_S = 10.4$ μs, $D_C = 2$ e^-/pixel/day (the lowest dark current measurement for the CCD running at 100K) and $\sigma_1 = 5.5$ e^- (from Fig. 10), a minimum background noise of 0.35 e^- with $N = 490$ is achieved. If the RN for one sample can be reduced to $\sigma_1 = 2$ e^- as it is expected with the use of new electronics, the minimum background noise achieved is about 0.21 e^- taking only $N = 178$ readings per pixel i.e., reading the whole detector in multiple sampling mode the minimum achievable noise of 0.21 e^- is obtained if each pixel is sampled 178 times.

This analysis shows the trade-off between RN and dark current at very deep sub-electron noise levels, and gives the perspective of the best performance achievable by the Skipper CCD.

5 Conclusions and future work

A readout technique for sub-electron noise level measurements was devised for a CCD imager fabricated on high resistivity silicon that is suitable for low background noise applications. This method is based on the capability of the Skipper CCD of performing several non-destructive measurements of the charge storage in each pixel. The noise and signal characteristics of the proposed readout system are derived, and compared to traditional methods used for typical CCDs (DSI).

Experimental results confirm the expected behaviour of the system. The Skipper CCD output stage transfer characteristic as well as another on-chip sources of noise as dark current, and horizontal and vertical CTI were analyzed, and their impact over the reduction of the readout noise was studied.

A RN of 0.2 e^- (RMS) was measured for a portion of the detector. Some hints for selecting the integration time and the number of samples of the readout system were given. Based on this result, the best expected performance for the operation of the complete detector was determined to be approximately 0.35 e^- RMS. In a near future, it is planned to use this technology to update the detector system of the Direct Dark Matter search using CCDs (DAMIC) experiment [20, 21].

It is also expected to develop new electronic hardware with lower noise levels. In the best scenario, this could improve the Skipper CCD performance up to 0.21 e^- RMS.

References

1. Boyle, W.S.: Nobel lecture: CCD—an extension of man's view. Rev. Mod. Phys. **82**(3), 2305–2306 (2010)
2. Smith, G.E.: Nobel lecture: the invention and early history of the CCD. Rev. Mod. Phys. **82** (3), 2307–2312 (2010)
3. Flaugher, B.: The dark energy survey instrument design. In: McLean, I.S., Iye, M. (eds.) Ground-based and Airborne Instrumentation for Astronomy. Proceedings of the SPIE, vol. 6269 (2006)
4. McLean, I.: Electronic Imaging in Astronomy—Detectors and Instrumentation, 2nd edn. Springer-Praxis, Berlin (2008)
5. Janesick, J.R.: Scientific Charge Coupled Devices. SPIE Publications, Bellingham, Washington (2001)
6. Chandler, C.E., et al.: Sub-electron noise charge coupled devices. SPIE Charge-Coupled Devices and Solid State Optical Sens. **1242**, 238–251 (1990)
7. Janesick, J.R., et al.: New advancements in charge-coupled device technology: sub-electron noise and 4096×4096 pixel CCDs. SPIE Charge-Coupled Devices and Solid State Optical Sens. **1242**, 223–237 (1990)
8. Holland, S.E., et al.: Fully depleted, back-illuminated charge-coupled devices fabricated on high-resistivity silicon. IEEE Trans. Electron. Dev. **50**(1), 225–238 (2003)
9. Wen, D.D.: Design and operation of a floating gate amplifier. J. Solid-State Circuits **SC-9**(6), 410–414 (1974)
10. Hynecek, J.: Low noise and high-speed charge detection in high-resolution CCD image sensors. IEEE Trans. Electron. Dev. **44**(10), 1679–1688 (1997)
11. Honscheid, K., DePoy, D.L.: The dark energy camera (DECam)-a new instrument for the dark energy survey. In: IEEE Nuclear Science Symposium Conference Record NSS '08, pp. 3357–3360 (2008)
12. Kandiah, K., Whiting, F.B.: Low noise charge sensing at the output of a CCD. IEE CCD workshop (1991)
13. Kandiah, K., Whiting, F.B.: Limits of resolution of charge sensitive detector systems. Nucl. Instrum. Methods Phys. Res. A **326**(1–2), 49–62 (1993). ISSN 0168-9002. doi:10.1016/0168-9002(93)90332-C
14. Estrada, J., et al.: Focal plane detectors for Dark Energy Camera (DECam). In: Proc. SPIE, vol. 7735, p. 77351R (2010)
15. Diehl, H.T., et al.: Characterization of DECam focal plane detectors. In: Dorn, D.A., Holland, D. (eds.) High Energy, Optical and Infrared Detectors for Astronomy III, Proceedings of the SPIE, vol. 7021, p. 70217 (2008)
16. Estrada, J., et al.: CCD testing and characterization for dark energy survey. In: McLean, I.S., Iye, M. (eds.) Ground-based and Airborne Instrumentation for Astronomy, Proceedings of the SPIE, vol. 6269, p. 62693K (2006)
17. Owens, A., Fraser, G.W., McCarthy, K.J.: On the experimental determination of the Fano factor in Si at soft X-ray wavelengths. Nucl. Instrum. Methods Phys. Res. A **491**(3), 437–443 (2002)
18. Fraser, G.W., et al.: The X-ray energy response of silicon Part A. Theory. Nucl. Instrum. Methods Phys. Res. A **350**(1–2), 368–378 (1994)
19. Janesick, J., et al.: Fano-noise limited CCDs. Proc. SPIE, vol. 982, p. 70 (1988)
20. Estrada, J., et al.: Prospects for a direct dark matter search using high resistivity CCD detectors. arXiv:0802.2872v3 [hep-ex] (2008). Accessed 1 Jul 2008
21. Barreto, J., et al.: Direct Search for Low Mass Dark Matter Particles with CCDs. arXiv:1105.5191v2 (2011)